Cement & Concrete Composites 43 (2013) 1–11

Contents lists available at SciVerse ScienceDirect

Cement & Concrete Composites

journal homepage: www.elsevier.com/locate/cemconcomp

Mixture design of self-compacting glass mortar

Sandra Nunes *, Ana Mafalda Matos, Tiago Duarte, Helena Figueiras, Joana Sousa-Coutinho

Laboratorio de Tecnologia do Betão e do Comportamento Estrutural, Departamento de Engenharia Civil, Faculdade de Engenharia, Universidade do Porto, rua Dr. Roberto Frias, 4200-465 Porto, Portugal

A R T I C L E   I N F O

Article history:
Received 6 September 2012
Received in revised form 15 April 2013
Accepted 26 May 2013
Available online 1 June 2013

Keywords:
A. Self-compacting concrete
Mortar
Glass powder
Statistical factorial design
Recycling

A B S T R A C T

Recycled ground glass is an unconventional material for self-compacting concrete (SCC). Nevertheless, its use is becoming increasingly attractive representing a twofold contribution to economic and eco-efficient SCC. In fact, on one hand mixed-color glass culets that are not reusable for packaging purposes may be employed. On the other hand its supplementary cementing potential can be used to replace expensive materials such as silica fume, metakaolin and cement, reducing CO_2 emissions. The present paper provides a comprehensive procedure for the design of SCC mortar mixtures incorporating fine glass powder. A central composite design was carried out to mathematically model the influence of mixture parameters and their coupled effects on deformability, viscosity, compressive strength, resistivity and resistance to carbonation. The derived models and a numerical optimization technique were used to select the best mixture, which maximizes durability and minimizes cost, while maintaining self-compactability.

1. Introduction

Sustainability is becoming a major selection criterion in new construction as businesses worldwide are attempting to build structures in a more eco-friendly manner. Civil engineers will be expected to exercise social responsibility by considering not only engineering properties and cost but also the ecological profiles of materials and durability of concrete structures at the designing stage [1,2]. In fact, in forthcoming codes, design for durability will have the same value as design for safety and serviceability. Producing structures that would function more efficiently over time, through the enhancement of durability is one of the ways by which the construction industry can become a part of the solution to the problem of sustainable development. Sustainable building development also includes a judicious use of resources, achieved by the use of industrial by-products and post-consumer discarded materials [1,2]. Concrete could be a viable solution to environmental problems since it allows incorporation of solid by-products from other industries. This would reduce the need to landfill these materials and the consumption of natural resources while still maintaining an acceptable, and sometimes even better, concrete quality [3]. In this line of research, LABEST/FEUP has been studying the feasibility of various recycled waste materials with cementing potential to be used in concrete like rice husk ash, biomass fly ash, forest waste bottom ash, waste from the paper pulp industry [4–7] and fine glass powder [8].

Glass is a major share of the total solid waste that is disposed daily worldwide. Due to the high cost of cleaning and color sorting, only a tiny proportion is either washed for reuse or re-melted to manufacture new glass. When the glass colors get mixed, most waste glass is sent to landfill as residue. Since glass is not biodegradable, landfills do not provide an environmental friendly solution, resulting in a growing interest in the recycling of waste glass [9,10]. A number of previous studies have examined the use of waste glass in concrete [11]. The use of waste glass as a raw material in the manufacture of Portland cement [12,13]; aggregate replacement [14–18], inert filler or partial cement replacement [9,17–25], has been investigated. However, most of the previous studies reported that the use of glass as a coarse aggregate has negative effects on mechanical properties, primarily because of a weak interface. Also, larger particle sizes of glass (greater than 1.2–1.5 mm) were found to facilitate alkali–silica reaction (ASR) in concretes [25,26]. ASR can be very detrimental to concrete unless appropriate actions are taken to minimize its effects. Such preventative actions include grinding glass, using suitable pozzolanic material such as fly ash, silica fume, metakaolin or ground blast furnace slag in the concrete mix in appropriate proportions, using alkali-resistant glass, using lithium additives, sealing concrete to keep it dry or using low alkali cement [9,14,18,22,27–29]. The coarse and fine glass aggregates could cause ASR in concrete, but the glass powder could suppress their ASR tendency, an effect similar to other supplementary cementitious materials (SCMs) [27].

* Corresponding author. Tel.: +351 225082121; fax: +351 225081835.
E-mail address: snunes@fe.up.pt (S. Nunes).

0958-9465/$ - see front matter © 2013 Elsevier Ltd. All rights reserved.
http://dx.doi.org/10.1016/j.cemconcomp.2013.05.009

Thus, most of the recent works have concentrated on milling glass cullet into powder form (glass powder) to replace cement in concrete [20,22–24]. The use of ground waste glass as cement replacement has also been investigated due to its pozzolanic properties [17,20–24]. Glass pozzolanic reactivity depends on the particle size. It was found that below 38 μm, glass is pozzolanic whereas between 38 and 75 μm glass has less or no pozzolanic property, and the finer the glass used the higher the concrete's strength especially at a late age [10,23,24]. Recent studies have investigated the influence of varying dosages of fine glass powder on cement hydration, and have modeled the degree of hydration of cement paste containing glass powder. Compared to fly ash concrete, concrete containing ground glass exhibited a higher strength at both early and late ages [24]. Fine glass powder was found to have the potential to improve some durability related properties of concrete. Fine glass powder, when used as a cement replacement material, besides reducing deleterious expansion due to alkali–silica reaction as stated, decreased both sorptivity and moisture diffusion coefficient [19,25]. Resistance to chloride transport is also improved by the use of this addition, indicating some amount of pore refinement [17,29].

Today, self-compacting concrete allows rethinking of the construction process due to its improved quality, productivity and working conditions. A self-compacting mixture has the ability to fill the form and consolidate under its own weight without any compaction energy. Placing has minimal dependence on available workmanship with great potential to improve quality of concrete in the final structure and to extend service life [30,31]. For self compacting concrete production, a high-volume of very fine material is necessary in order to make the concrete more fluid and cohesive. Self-compactibility of concrete is generally achieved by using a certain amount of very fine particles like fly ash, limestone filler or granulated blast furnace slag, in addition to cement. Nevertheless, limited work has been carried out on the application of ground glass in SCC. Studies on self-consolidating glass concrete mixtures proceeded by trial and error, using conventional single factor experiments [10,14,19,26]. However, for a concrete mixture (containing six or more constituent materials) which must meet several performance criteria (e.g. self-compactability, compressive strength, rapid chloride permeability, carbonation), simultaneously, trial and error or "one factor at a time" approaches will be inefficient and costly. More importantly, they may not provide the best combination of materials at minimum cost. A better approach to design concrete mixtures is to conduct a Factorial Design experiment. This is a design approach that refers to the process of planning the experiment so that appropriate data can be analyzed by statistical methods, resulting in sound conclusions with a minimum number of experiments. A statistical design approach offers a valid basis for developing an empirical model that is an equation derived from data that expresses the relationship between the response and the important design factors. This empirical model can then be manipulated mathematically for various purposes, for example, mixture optimization [32]. Since mortar properties, adequate for SCC, were sufficiently well defined during the early development of SCC, at the University of Tokyo, by Prof. Okamura and his co-workers [33], initial tests can be carried out at mortar level [34].

The aim of the present paper is to explore the feasibility of using recycled ground glass powder in self-compacting concrete (SCC). The ground glass was used as a partial replacement for cement. A factorial experimental plan was used to establish numerical models relating mixture parameters to spread flow, flow time, resistivity and carbonation depth of mortar. The derived numerical models were used first to find solutions adequate for SCC, within the experimental domain, i.e. mixtures which exhibit both a spread flow of 260 mm and a flow time of 10 s. Then, the optimum SCC mortar mix was selected as that mix which maximizes durability while minimizing cost.

2. Experimental programme

2.1. Materials characterization

The mortar mixes investigated in this study were prepared with a typical commercial Type I Portland cement that complies with the requirements of NP EN 197-1:2001, fine glass powder (GP), reference sand conforming to CEN EN 196-1:2006 and tap water. The chemical and relevant physical properties of cement and glass powder are presented in Table 1. The SiO_2 and ($Na_2O + K_2O$) of GP are much higher than those of cement. The total reactive component ($SiO_2 + Al_2O_3 + Fe_2O_3$) contents of glass are about the same as those of a typical fly ash [10]. Waste glass was obtained from a recycling glass industry, in Portugal, where waste glass such as car windscreen glass is crushed and sold to the container glass industry. Fine waste glass from this industry was ground in a ball mill in the laboratory. The particle size distribution of GP and cement, measured by using a laser particle size analyzer, are shown in Fig. 1. A commercially available polycarboxylate type superplasticizer (SikaViscocrete 3006 ®) was used having a specific gravity of 1.05% and 18.0% solids content. Reference sand was a siliceous round grain natural sand (0.08–2 mm) with a specific gravity of 2.57 and an absorption value of 0.68% by mass.

The morphology of glass powder was examined under a scanning electron microscope (SEM). Glass powder was spread on a conductive double-edged adhesive tape and stuck to a SEM sample stud. Loose particles were dislodged with a blast of air. The samples were extensively viewed and then representative photographs were taken. It was observed that glass powder from the grinding process consist mainly of fine angular particles with a narrow particle size range, as shown in Fig. 2.

2.2. Preliminary tests

Alkali–silica reactivity (ASR) is a chemical reaction between Portland cement concrete and certain aggregates. This reaction produces a gel (see Fig. 3), which is expansive and could cause premature cracking in concrete, thereby causing severe damage in concrete structures or can accelerate the progress of other

Table 1
Chemical and physical properties of cement (CEM I 42.5R) and glass powder (GP).

	CEM I 42.5R	GP
SiO_2 (%)	20.36	70
AL_2O_3 (%)	5.1	1.2
Fe_2O_3 (%)	3.12	0.65
CaO (%)	62.72	8.7
MgO (%)	1.81	3.7
SO_3 (%)	3.44	<0.05
Na_2O (%)	–	16
K_2O (%)	–	0.35
Na_2O eq.(%)	0.8	16.23
Cl (%)	0.012	<0.005
Free CaO (%)	1.62	
Loss on ignition (%)	2.61	0.92
Insoluble residue (%)	1.33	
Specific density (g/cm^3)	3.16	2.39
fc (MPa) (mortar prisms)		
7 d	40	
28 d	52	
Vicat test		
Initial set (min)	150	
Final set (min)	205	

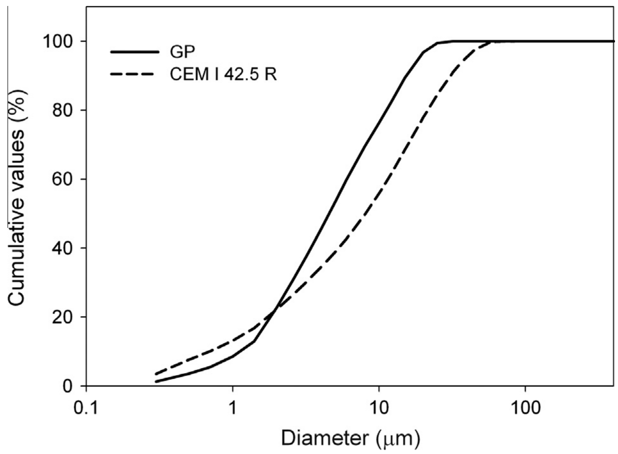

Fig. 1. Particle size distribution of CEM I 42.5 R and glass powder.

reactions that in turn cause damage, such as freeze–thaw or corrosion. This phenomenon, however, takes many months and requires favorable conditions such as high moisture and temperatures in excess of 40 °C before being noticed. Glass, due to its silica-rich nature and amorphous structure, is susceptible to chemical attack under the high alkali conditions provided by the hydrated cement phase in the concrete [9].

The potential of expansion due to alkali–silica reaction of the glass powder used in this study was investigated using an accelerated mortar bar method (slightly modified from ASTM C1547). A reactive siliceous sand (CEN EN 196-1:2006) was used as the aggregate. Two $25 \times 25 \times 275$ mm^3 mortar bars were cast for each batch. The mortar mixtures had an aggregate-to-cementitious material ratio of 3 and a water-to-cementitious material ratio of 0.5, differing from those indicated in ASTM C1547 of 2.25 and 0.47, respectively. Immediately after casting, the specimens with molds were taken into a moisture room at 23 ± 2 °C and covered with a plastic sheet. They were demolded 24 ± 2 h after the casting and preconditioned for a further 24 h in water maintained at 80 ± 2 °C. The lengths of these mortar bars after immersion in the hot water were measured as initial lengths, and then the mortar bars were subsequently transferred to 1 N NaOH solution maintained at 80 ± 2 °C and periodically measured for 26 d.

For the ASR study, GP was used to replace 10%, 20%, 30%, 40% and 50% of the cement in the mortar mixtures. In Fig. 4 length change with time is presented, as an average of two identical mortar bars at each age. After 14 d, the expansion of the plain mortar mixture was 0.24%, and 0.38% after 26 d. From Fig. 4, it could be observed that an increase in glass powder content reduces the expansion of mortar. Nevertheless, the reduction in expansion (at the end of 14 or 26 d) was not found to be proportional to the replacement level of cement with glass powder. For this particular aggregate, more than 20% replacement of cement by glass powder will be required to limit the expansion below 0.10%. A specific cement and a particular aggregate, in combination, demonstrate a certain behavior in terms of ASR providing a specific expansion in a standardized test. Findings by other authors [9,23,25] have proved that glass powder can suppress the ASR tendency of reactive aggregates with which present results are in accordance.

2.3. Experimental design

In the present study experiments were designed according to a central composite design adequate to fit a second order model [32]. This design consisted on a 2^3 factorial statistical design (three factors at two levels) augmented with 6 axial runs plus 5 central runs to evaluate the experimental error. The generic form of a second order model is:

$$y = \beta_0 + \sum_{i=1}^{k}\beta_i x_i + \sum_{i=1}^{k}\beta_{ii}x_i^2 + \sum_{i<j}\sum \beta_{ij}x_i x_j + \varepsilon \quad (1)$$

where y is the response of the material; x_i are the independent variables; β_0 is the independent term; β_i, β_{ii} and β_{ij} are the coefficients of independent variables and interactions, representing their contribution to the response; ε is the random residual error term representing the effects of variables or higher order terms not considered in the model.

For mortar (or concrete), the sum of volume fractions of the various mixture components is constrained to sum up to one. Therefore, the volume fractions cannot be taken directly as variables in a factorial experiment because they are not independent. One viable option is to reduce q mixture components to $(q-1)$ independent factors by taking the ratio of two components (whether in volume or weight fractions). In the present study SCC mortar mix proportions were established based on the following variables x_i: water to powder volume ratio (V_w/V_p); water to cement weight ratio (w/c); superplasticizer to powder weight ratio (Sp/p); sand to mortar volume (V_s/V_m), as suggested by Okamura et al. [33]. Sand to mortar volume ratio was kept constant and equal to 0.475. The effect of the remaining variables was evaluated at five different levels $-\alpha$, -1, 0, +1, $+\alpha$ as presented in Table 2. In order to make the

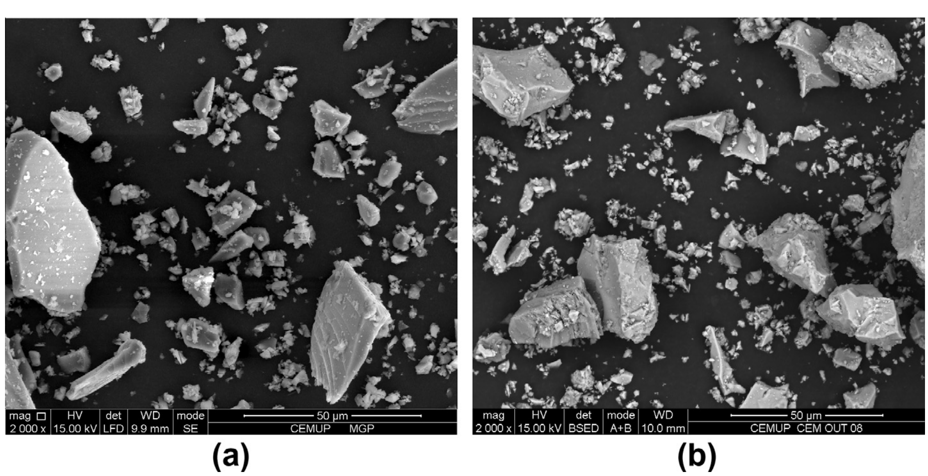

Fig. 2. Particle morphology of (a) glass powder and (b) cement (×2000).

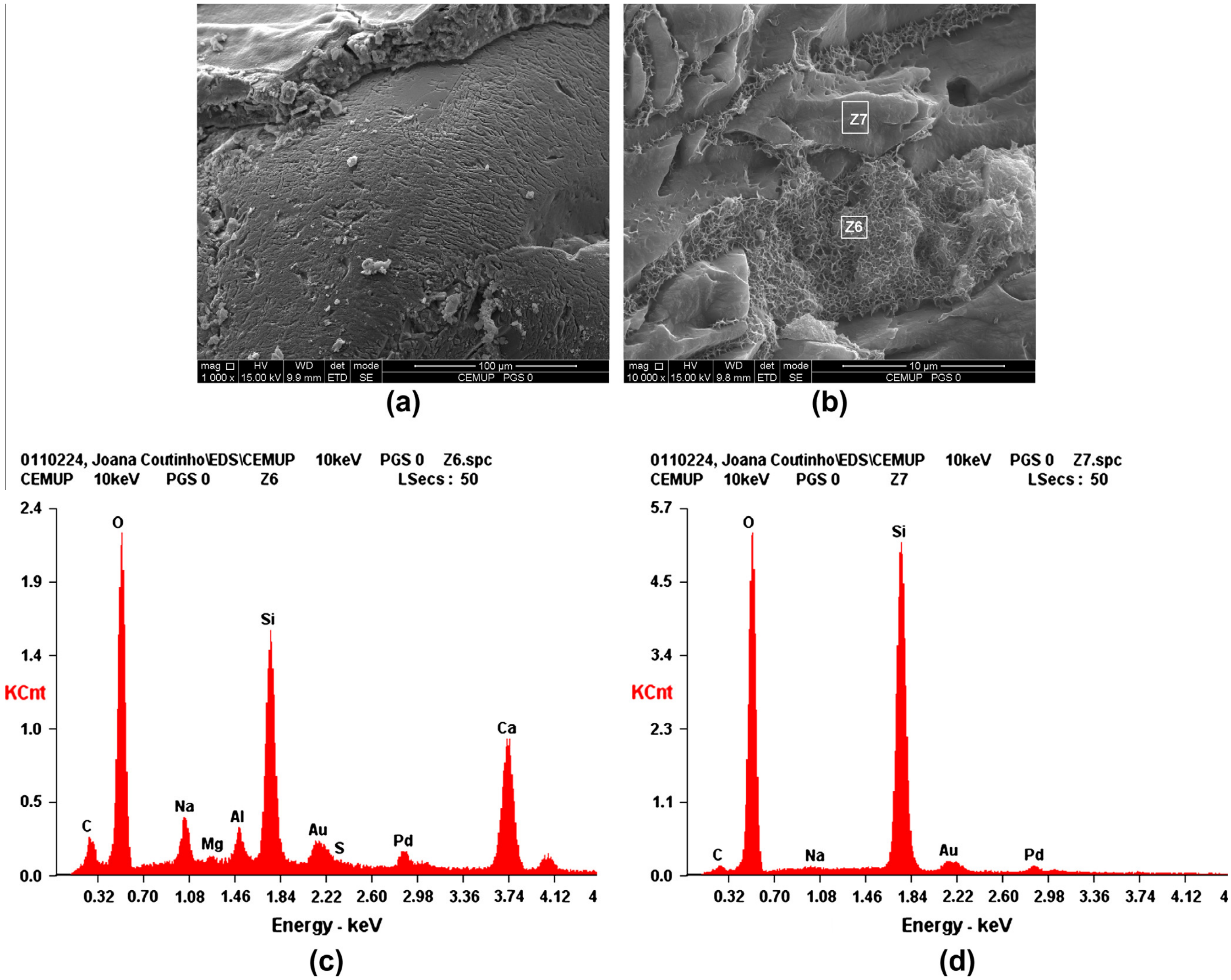

Fig. 3. SEM images and XRD diffraction analysis: (a) site of ASR gel formation over a sand particle; (b) location of zones Z6 (gel) and Z7 (sand particle); (c and d) XRD diffraction analysis of material in zones Z6 and Z7, respectively.

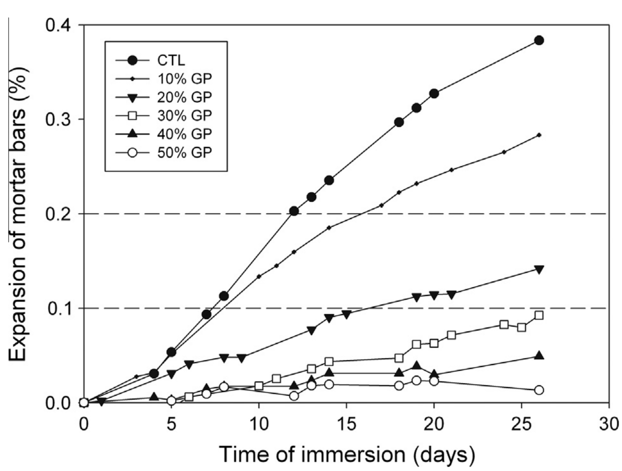

Fig. 4. ASR expansion of mortar bars.

Table 2
Coded values for the variables used in the experimental design.

Ref.	Point type	V_w/V_p	w/c	Sp/p
Ci[a]	Central	0	0	0
F1	Factorial	−1	−1	−1
F2	Factorial	1	−1	−1
F3	Factorial	−1	1	−1
F4	Factorial	1	1	−1
F5	Factorial	−1	−1	1
F6	Factorial	1	−1	1
F7	Factorial	−1	1	1
F8	Factorial	1	1	1
CC1	Axial	−1.682	0	0
CC2	Axial	1.682	0	0
CC3	Axial	0	−1.682	0
CC4	Axial	0	1.682	0
CC5	Axial	0	0	−1.682
CC6	Axial	0	0	1.682

[a] Central point was replicated five times.

design rotatable (i.e. the standard deviation of the predicted response is constant in all points at the same distance from the center of the design) the α value should be taken equal to $F^{1/4}$, where F is the number of points in the factorial part of the design [32]. In the case treated in this paper, this corresponds to taking α equal to 1.682. The parameters β_0, β_i, β_{ii} and β_{ij} of the models are

Table 3
Correspondence between coded values and actual parameter values.

Mixture parameter	−1682	−1	0	+1	+1682
V_w/V_p	0.732	0.800	0.900	1.000	1.068
w/c	0.40	0.44	0.50	0.56	0.60
Sp/p	1.17%	1.20%	1.25%	1.30%	1.33%

estimated by regression techniques and are valid for mixtures made within the range of values presented in Table 3.

In this work, experimental mixtures F1 and F8 (see Table 2) were assessed first and their results were analyzed before proceeding with the rest of the experimental plan, in an attempt to check the adequacy of the selected range of mixture parameters. Considering the combination of mixture levels in the F1 and F8 mixes, these should respectively lead to one of the least fluid mixtures and to one of the most fluid mixtures, of all mixtures in the experimental plan. Thus, it is desirable that the interval formed by the results obtained from F1 and F8 mixtures includes the target value for each mortar test which are a spread of 260 mm and a flow time of 10 s, in the present work. When this is not the case, the range of one or more variables should be changed. The final mix proportions of each tested mix are presented in Table 4, where the replacement percentage of cement by glass powder ranges from 22% to 47%.

2.4. Mixing sequence, testing methods and test results

With the exception of F1 and F8, the run order was randomized to reduce effects of extraneous variables not explicitly included in the experiment. The mixes were prepared in the laboratory in 1.4 l batches and mixed in a two-speed mixer complying to NP EN 196-1:1996. The mixing sequence consisted of mixing sand and powder materials with 0.81 of the mixing water during 60 s, stopping the mixer to scrape material adhering to the mixing bowl, mixing for another 60 s, adding the rest of the water with the superplasticizer, mixing for 60 s, stopping the mixer again to scrape adherent material, mixing for 30 s, stopping the mixer for 1 min and finally mixing mortar during a further 30 s. The mixer was always set at low speed except in the last 30 s of the mixing sequence where it was set at high speed. Mortar tests using the flow cone and the V-funnel, with the same internal dimensions as the Japanese equipment, were then carried out to characterize fresh state (see [33] for details on equipments and test procedures). The mortar flow test was used to assess deformability by calculating the flow diameter as the mean of two diameters in the spread area. The V-funnel test was used to assess the viscosity and passing ability of the mortar. Test flow time was recorded. After the fresh mortar tests six ($40 \times 40 \times 160$ mm^3) prisms were molded: three to evaluate resistivity over time up to 90 d; two to evaluate compressive strength at 28 d; and one to evaluate resistance to carbonation. Mortar specimens were demolded 1 d after casting and kept under water in a chamber under controlled environmental conditions (Temp. = 20 °C and RH = 95–98%) until testing age.

A range of microstructural properties can be evaluated by electrical measurements, including porosity, pore connectivity, water permeability, and ion diffusivity [35]. Resistivity is an intrinsic property of the material that relates to the ability of concrete to carry electric charge and it depends mainly on the hydration process (nature and topography of pore structure), changes in pore solution composition, moisture and temperature conditions. Electrical resistivity of water saturated concrete provides indications on the pore connectivity and therefore, on the concrete resistance to penetration of liquid or gas substances, thus resistivity is a parameter which accounts for the main key properties related to concrete durability [36]. Regarding the influence of the chemical composition of pore solution, Andrade [36] stated that its impact in the total resistivity is small providing the concrete remains alkaline. At high pH values the pore solution resistivity varies from 0.3 to 1.0 Ω m, which is comparatively very small taking into account that mortar resistivity after several days of hardening is in the range of a few dozen Ω m. Rajabipour and Weiss [35], also found in their work that the moisture connectivity is the single most important parameter governing the overall conductivity of a cement paste specimen. The pore solution conductivity and the volume fraction of moisture have a far lower influence on the overall conductivity. However some studies called attention to the fact that the replacement of Portland cement with supplementary cementing materials, such as silica fume, can increase the electrical resistivity of concrete due to the change in the chemical composition of the pore solution [37]. In the present work, resistivity was assessed by the two electrodes technique on prismatic specimens ($40 \times 40 \times 160$ mm^3) in which stainless steel networks were

Table 4
Mix proportions and properties of fresh and hardened mortar specimens.

Mix number	Ref.	W_c (kg/m^3)	W_{GP} (kg/m^3)	W_w (kg/m^3)	W_{sp} (kg/m^3)	W_s (kg/m^3)	Dflow (mm)	Tfunnel (s)	fc, 28 d (MPa)	Resistiv, 28 d (Ω m)	Carb (mm)
1	C1	497.4	276.9	244.5	9.68	1249.3	269.25	7.37	67.5	256.4	0.0
2	C2	497.4	276.9	244.5	9.68	1249.3	284.25	7.89	55.5	252.1	2.1
3	C3	497.4	276.9	244.5	9.68	1249.3	284.50	7.27	65.9	241.1	1.5
4	C4	497.4	276.9	244.5	9.68	1249.3	294.75	6.55	65.4	256.3	1.5
5	C5	497.4	276.9	244.5	9.68	1249.3	321.50	6.38	65.4	225.2	1.8
6	F1	529.7	288.7	229.0	9.82	1249.3	158.00	29.80	78.3	345.8	0.0
7	F2	595.9	168.0	258.7	9.17	1249.3	293.00	4.62	71.9	105.1	0.0
8	F3	417.1	375.5	229.3	9.51	1249.3	231.75	14.38	56.9	408.0	4.1
9	F4	469.2	265.6	259.0	8.82	1249.3	354.00	3.22	65.3	214.1	4.2
10	F5	529.7	288.7	228.4	10.64	1249.3	199.75	17.22	71.0	288.4	0.0
11	F6	595.9	168.0	258.1	9.93	1249.3	311.75	4.70	72.9	88.3	0.0
12	F7	417.1	375.5	228.6	10.30	1249.3	351.00	8.72	66.9	287.5	3.0
13	F8	469.2	265.6	258.4	9.55	1249.3	350.75	3.26	67.7	192.6	3.9
14	CC1	443.7	382.4	217.1	10.33	1249.3	178.00	31.33	76.7	504.4	0.3
15	CC2	542.3	188.6	267.4	9.14	1249.3	358.25	2.64	66.6	105.7	2.1
16	CC3	621.7	181.1	244.2	10.03	1249.3	253.75	9.05	77.9	125.5	0.0
17	CC4	414.5	340.8	244.7	9.44	1249.3	349.75	5.33	57.4	144.5*	5.1
18	CC5	497.4	276.9	245.0	9.03	1249.3	284.00	7.54	53.7	201.9	2.6
19	CC6	497.4	276.9	244.0	10.33	1249.3	317.00	6.28	62.8	225.6	2.9

W_c, W_{GP}, W_{sp}, W_w, W_s represent the weight (by unit of mortar volume) of cement, glass powder, superplasticizer, free water and sand, respectively.

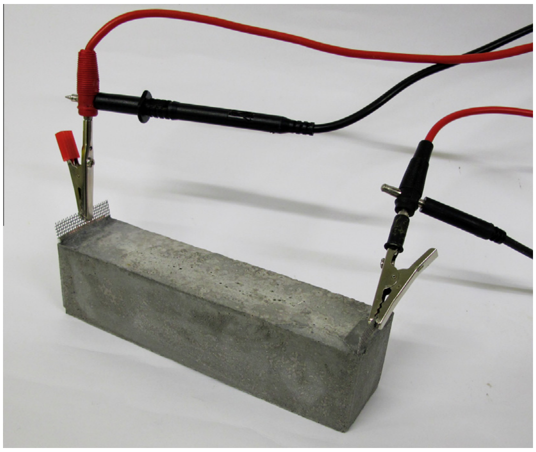

Fig. 5. Mortar resistivity measuring set-up.

embedded to work as electrodes (see Fig. 5) [38]. Applying Ohm's Law, as shown in Eq. (2), the relationship between the intensity of the applied current and the potential difference measured gives the electrical resistance of the material. The resistivity is obtained applying to the electrical resistance a geometric factor, which depends on the geometrical dimensions of the specimen and the electrodes used.

$$R = V/I = \rho \cdot (L/A) \Rightarrow \rho = V \cdot A/(L \cdot I) \quad (2)$$

where R is the electric resistance, (Ω – Ohm); I, current (Amp.); V, voltage (Volts); ρ, electric resistivity (Ω m); L, length (m); and A (m^2) the cross area of the test specimen through which current passes. Since all the specimens were at the same moisture (saturated) and temperature conditions, the resistivity measure can be used to compare the porous structure of various mortar specimens and therefore constitute a measure of the amount and interconnectivity of the cementitious matrix pores. This test was selected because it is a very simple, rapid and non-destructive test, enabling the use of the same specimens to assess other properties, such as the compressive strength.

Resistance to carbonation was evaluated generally following the procedure described in the Portuguese specification LNEC E 391 [39]. The samples were subjected to wet curing for 28 d, and then were stored in a room with controlled temperature and relative humidity (20 ± 0.3 °C and 50 ± 3%, respectively) during 14 d. Then, specimens were exposed to 5 ± 0.1% carbon dioxide, relative humidity of 60 ± 5% and temperature of 23 ± 3 °C, in an accelerated carbonation chamber. Specimens used were sawn off the ends of ($40 \times 40 \times 160$ mm^3) prisms. Carbonation depth (Carb) was evaluated after about 60 d of exposure in the accelerated carbonation chamber.

The average test results of spread flow diameter (Dflow), flow time (Tfunnel), compressive strength at 28 d (fc, 28), resistivity at 28 d (Resistiv, 28 d) and carbonation depth (Carb) after 60 d of exposure for each mix are shown in Table 4. From the statistics presented in Table 5 it may be observed that with this experimental plan a wide range of mortars was covered and the range of Dflow and Tfunnel results obtained is adequate, since it includes both targets Dflow and Tfunnel.

3. Response models

In this work commercial software (Design-Expert) [40] was used to analyze the results for each response variable, by examining summary plots of the data, fitting a model using regression analysis and analysis of variance (ANOVA), validating the model by examining the residuals for trends and outliers and, finally, interpreting the model graphically. The statistical analysis is described in detail for Dflow. The analysis of the other response variables was performed in a similar manner.

3.1. Model identification and validation

The first step in the analysis is to identify a plausible model. The design selected permits estimation of a full quadratic model (see Eq. (1)). The model parameters (β_0, β_i, β_{ij}) are estimated by means of a multilinear regression analysis. Nevertheless, it may happen that some of the terms in Eq. (1) may not be significant. The significance of each factor on a given response can be evaluated using a Student's t-test. In the present work, a step-by-step backward elimination was used to eliminate non-significant terms in the regression model (the criteria used for the entry and removal of a variable in the model was $\alpha < 0.05$ and $\alpha > 0.10$, respectively) [40]. ANOVA is used to evaluate the regression model in several aspects, namely, the significance of regression, lack of fit and significance of each variable in the model. The ANOVA results derived from the Dflow data set is shown in Table 6. The Model F-value of 26.20 implies the model is significant. The lack of fit F-statistic of 1.03 implies that the lack of fit is not significant relative to the pure error. Table 6 also shows that only significant terms were included in the model. The resulting model for Dflow, in terms of actual variables, was

$$\begin{aligned}\text{Dflow} = {} & -6987.45 + 8218.75V_w/V_p + 2964.07\text{w/c} \\ & + 361350.49\text{Sp/p} - 2627.80(V_w/V_p \times \text{w/c}) \\ & - 363750.00(V_w/V_p \times \text{Sp/p}) - 1036.56(V_w/V_p)^2 \quad (3)\end{aligned}$$

The corresponding estimated model coefficients, in terms of coded variables, including the respective residual standard deviation, along with the correlation coefficients, are given in Table 7. The values of both R^2 and R^2_{adj} close to 1.0 indicate that a large proportion of the variability of Dflow response is explained by

Table 5
Statistics of the results for the total points and for central points.

	Minimum	Maximum	Mean	Standard deviation	Coefficient of variation (%)
N = 5 central points					
Dflow (mm)	269.25	321.50	290.85	19.40	6.7
Tfunnel (s)	6.38	7.89	7.09	0.62	8.8
fc, 28 d (MPa)	55.5	67.5	63.9	4.8	7.5
Resistiv, 28 d (Ω m)	225.2	256.4	246.2	13.3	5.4
Carb (mm)	0.0	2.1	1.4	0.8	59.3
N = 19 total points					
Dflow (mm)	158.00	358.25	285.62	61.72	21.6
Tfunnel (s)	2.64	31.33	10.10	8.83	87.4
fc, 28 d (MPa)	53.7	78.3	66.6	7.2	10.9
Resistiv, 28 d (Ω m)	88.3	504.4	235.2	105.5	44.9
Carb (mm)	0.0	5.1	1.8	1.7	91.4

Table 6
Anova tests.

Tests for	Source	Sum of squares	Degrees of freedom	Mean square	F value	p-value (prob > F)
Significance of regression	Model	60472.34	6	10078.72	26.20	<0.0001
	Residual	4616.92	12	384.74		
	Total	65089.26	18			
Lack of fit	Lack of fit	3111.84	8	388.98	1.03	0.5245
	Pure error	1505.08	4	376.27		
Partial significance of each predictor variable	V_w/V_p	33080.56	1	33080.56	85.98	<0.0001
	w/c	17327.24	1	17327.24	45.04	<0.0001
	Sp/p	3941.14	1	3941.14	10.24	0.0076
	$(V_w/V_p) \times$ (w/c)	1953.12	1	1953.12	5.08	0.0438
	$(V_w/V_p) \times$ (Sp/p)	2646.28	1	2646.28	6.88	0.0223
	$(V_w/V_p)^2$	1523.98	1	1523.98	3.96	0.0698
	Residual	4616.92	12	384.74		

Table 7
Fitted numerical models (coded variables).

Response variable Model terms	Dflow (mm) Estimate	[Tfunnel (s)]$^{-0.5}$ Estimate	[Resistiv, 28 d (Ω m)]$^{-0.5}$ Estimate	Carb (mm) Estimate
Independent	294.030	0.3827	0.0651	1.285
V_w/V_p	49.217	0.1279	0.0155	0.301
w/c	35.620	0.0390	−0.0085	1.732
Sp/p	16.988	0.0134	NS	−0.068
$(V_w/V_p)\times$(w/c)	−15.625	NS	−0.0074	NS
$(V_w/V_p)\times$(Sp/p)	−18.188	−0.0176	NS	NS
$(V_w/V_p)^2$	−10.366	NS	0.0020	NS
$(w/c)^2$	NS	NS	0.0035	0.355
$(Sp/p)^2$	NS	NS	NS	0.423
Residual error, ε*				
Mean	0	0	0	0
Standard deviation	19.61	0.014**	0.0036**	0.622
$R^2/R^2_{adjusted}$	0.93/0.89	0.99/0.99	0.97/0.96	0.90/0.86

(NS) non-significant terms.
* Error term is a random and normally distributed variable and no evidence of autocorrelation was found in the residues.
** Corresponding value for (Tfunnel) and (Resistiv, 28 d) is 1.28 and 31.51, respectively.

Table 8
Tests on residuals.

Test	Statistic	Degrees of freedom	Significance
Kolmogorov–Smirnov[a]			
Unstandardized residual	0.166	19	0.177
Studentized residuals	0.169	19	0.156
Shapiro–Wilk			
Unstandardized residuals	0.955	19	0.474
Studentized residuals	0.952	19	0.427
Durbin–Watson	1.574		

[a] Lilliefors significance correction.

the obtained regression model. A value of residual standard deviation near the experimental error (given by replicate standard deviation in Table 5) is an indication of an adequately fitting model. The replicate standard deviation value is 19.40, which is very close to 19.61.

The hypothesis testing involved in regression analysis is based on the assumptions that the errors are independent and normally distributed with zero mean and constant variance. In the present work the Normal probability plot of residuals (unstandardized, standardized and studentized residuals) were examined to check normality, the plots of residuals against predicted values and the plot of residuals against values of the individual predictor variables were analyzed to check the constancy of residual variance. In addition, the Kolmogorov–Smirnov Lilliefors and Shapiro–Wilk tests for normality were performed (see Table 8). Analysis of all of these plots (not included here due to limitations of space) and test statistics did not reveal obvious model inadequacies or indicate serious violations of the normality assumptions. The Durbin–Watson test statistic was used to detect the presence of autocorrelation in the residuals from the regression analysis. The test statistic is compared to lower (Q_L) and upper (Q_U) critical values, which vary by level of significance, the number of observations, and the number of predictors in the regression equation. For a 5% level of significance, 19 observations and 6 predictor variables, one obtain $Q_L = 0.751$ and $Q_U = 2.022$. Since Durbin–Watson test statistic is in between Q_L and Q_U, this test was inconclusive. Nevertheless, the randomness of residuals was confirmed by computing autocorrelations for data at varying time lags. Autocorrelations were found to be near zero for all time-lag separations.

Another important issue is the detection of regression outliers which can have a harmful influence in the process of fitting the model to the data. Identification of outliers for their eventual removal from the dataset, was carried out by analyzing the Cook's distance. If there are no outliers, these distances are of approximately equal amplitude and less than 1.0 [32]. For the current Dflow model, the maximum value of the Cook distance measure was 0.80.

Once a valid model is obtained, it can be interpreted graphically using response surface and contour plots. Because these plots can only show two variables at a time (the other variables are set at fixed conditions), several plots must be examined. Fig. 6 exemplifies a surface plot of Dflow as a function of w/c and V_w/V_p, with the other variable (Sp/p) fixed at the central value. From this plot it is possible to clearly identify conditions which give optimum Dflow response (260 mm). This plot also indicates that V_w/V_p has a larger influence on Dflow as compared to w/c and the existence

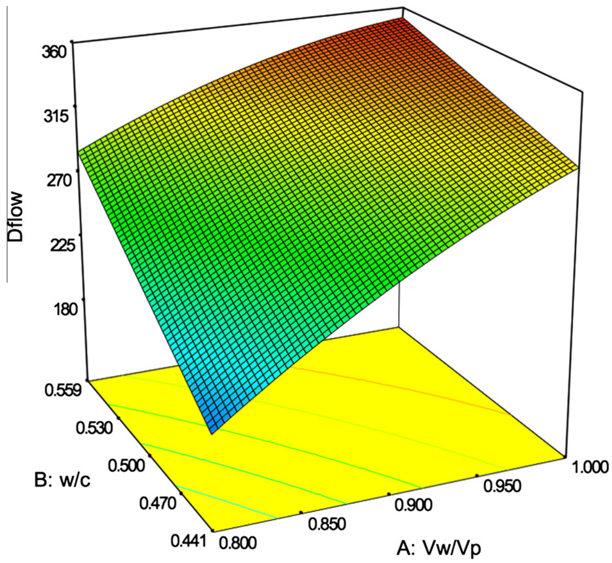

Fig. 6. Dflow surface plot (Sp/p = 1.25%).

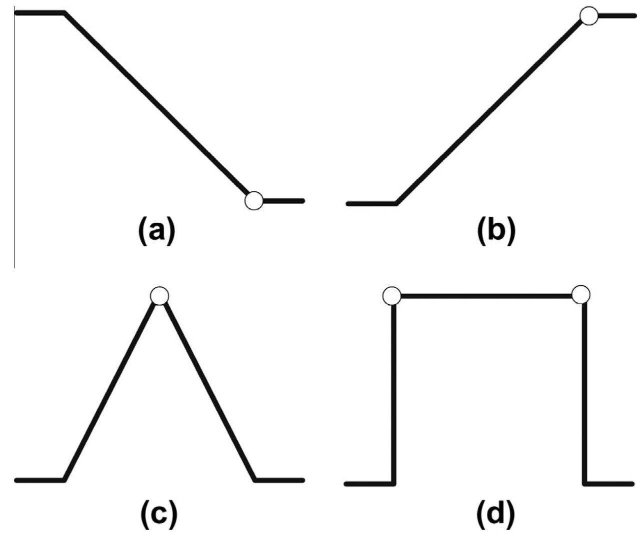

Fig. 7. Desirability functions for optimization: (a) to minimize; (b) to maximize; (c) to target a specific level; and (d) to keep within a specified range.

of an interaction effect between w/c and V_w/V_p (this will be further discussed in Section 3.3).

3.2. Models for other responses

Using the same procedure described above for Dflow the models presented in Table 7 were fitted to Tfunnel; Resistiv, 28 d; and Carb. A variable transformation of the form $1/\sqrt{y}$ was used for modeling of both Tfunnel and Resistiv, 28 d in order to stabilize the response variance and improve the fit of the model to the data. Notice that the observed value of 144.5 in the variable Resistiv, 28 d (marked with * in Table 4) is not typical of the rest of the data. This value was identified as an outlier in the statistical analysis and for this reason it has been excluded from the data when fitting the model. For the materials and conditions of this experimental plan a relatively small variation was found for fc, 28 d results (10.9%) as compared to the experimental error (7.5%) (see Table 5); for this reason no adequate model was found to fit fc, 28 d response.

3.3. Individual and interaction effects

The estimates of the model coefficients presented in Table 7, obtained for the coded variables, give an indication of the relative significance of the various mixture parameters on each response. Naturally a negative coefficient means that the response variable will decrease if the given mixture parameter increases. The results in Table 7 clearly show that V_w/V_p exhibited a great effect on all responses, being only exceeded by the effect of w/c on Carb response It should be noted that (w/c) and (V_w/V_p) are related to the glass powder to cement weight ratio (GP/c) as follows

$$GP/c = \left[\left(\frac{w/c}{\rho_w \times \frac{V_w}{V_p}}\right) - \frac{1}{\rho_c}\right] \times \rho_{GP} \tag{4}$$

where ρ_w, ρ_c and ρ_{GP} represent the specific gravity of water, cement and glass powder, respectively. Thus, the substitution of cement by glass powder (an increase of Gp/c) while maintaining the volume of fines and water content represents a reduction of w/c ratio which has a strong negative influence on carbonation, based on results from Table 7. Nevertheless, an increase of GP/c while maintaining the w/c ratio represents a reduction of V_w/V_p, which has a strong influence on the workability of mortars, reducing the flow diameter and increasing the flow time, but significantly improves its microstructure, by increasing the resistivity. Jain et al. [29] observed that glass powder, which has a high Na_2O content, releases a small fraction of alkalis into the pore solution, thus increasing the conductivity of the pore solution. Even with such increase, pastes with GP presented higher resistivity.

Besides V_w/V_p, the variable that most influenced Dflow, (Tfunnel)$^{-0.5}$ and (Resistiv, 28 d)$^{-0.5}$ was w/c. Significant interaction effects were found between V_w/V_p and Sp/p on both responses related to the fresh state. In addition, an interaction effect between V_w/V_p and w/c was found to be significant on Dflow response. Other quadratic terms on V_w/V_p, w/c and Sp/p were also found to be significant for the mortar responses, as shown in Table 7.

4. Mixtures optimization

The desirability function approach is used in the commercial software (Design-Expert) [40] for the simultaneous optimization of one or more goals. First, a desirability function must be defined for each of the independent and dependent variables. The desirability function takes values between 0 and 1, and may be defined in several ways (see Fig. 7). The allowable goals are to minimize or maximize a variable, to target a specific level of a variable; to keep a variable within a specified range or none (the default goal is to keep the variable within the low and high limits) [40]. Each goal is assigned as a weight (number between 1 and 5 with 5 being the most important and 1 the least important). The individual desirabilities are then combined using the geometric mean, which gives an overall desirability function. The optimization software searches for the greatest overall desirability. A value of one of the desirability function represents the ideal case. A zero indicates that one or more responses fall outside desirable limits. The goal seeking begins at a random starting point and proceeds up the steepest slope to a maxima. There may be two or more maxima because of curvature in the response surfaces and their combination into the desirability function. Therefore, starting from several points in the desiring space may be necessary to find the best local maximum.

4.1. Solutions for SCC mortars

After building the regression models that establish relationships between mix design variables and the responses, the numerical optimization technique was used to determine the range of mortar mixture parameters where deformability and viscosity coexist in a balanced manner, i.e. to determine the best mixtures which exhibit a spread flow of 260 mm and a flow time of 10 s, based on previous experience of the authors [34]. The values of V_w/V_p and Sp/p that can lead to the best mixtures were searched for each w/c value, by using the following goals (having equal importance weights)

$$\begin{cases}\text{target Dflow is 260 mm}\\\text{target Tfunnel is 10 s}\end{cases}.$$

and the restriction

$$\text{w/c equal to } a; \text{ with } a \text{ varying from 0.4 to 0.58 by steps of 0.01} \quad (6)$$

At this stage, no restriction was established for the other response variables. Note that since the response models were expressed as a function of three independent variables, a multiple optimum will hardly occur. Because the error in predicting the responses increases with the distance from the center of the modeled region, the use of the models was limited to an area bound by coded values +2.3 to −2.3. The adjusted values of V_w/V_p and Sp/p for each pair of w/c are presented in Fig. 8. The corresponding values for estimated mortar resistivity, at 28 d, and carbonation depth are presented in Figs. 9 and 10, respectively. Maximum estimated value of resistivity for SCC mortars incorporating GP, at 28 d, is about 314 Ω m. Figueiras et al. [38] found similar resistivity results, at 28 d, for mortars including ternary mixtures of CEM I 42.5 R + limestone filler + metakaolin. It is worth mentioning that mortar resistivity increases further beyond the age of 28 d, as can be observed in Fig. 11. Thus, glass powder significantly improved mortars durability, having a great potential to replace expensive imported materials, like silica fume or metakaolin, and making high-performance SCC mixtures more economic.

4.2. Selection of optimum SCC mortar mix

The optimum SCC mortar mix is defined here as that mix which maximizes durability while minimizing cost (by means of a higher w/c ratio). Thus, by adding the following goals

$$\begin{cases}\text{maximize Resistiv, 28 d}\\\text{minimize Carb, 28 d}\\\text{maximize w/c}\end{cases}$$

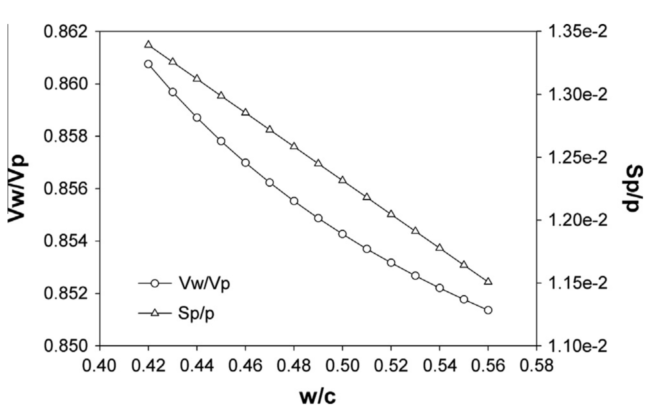

Fig. 8. Adjusted mixture variables (actual values) for optimized SCC mortars.

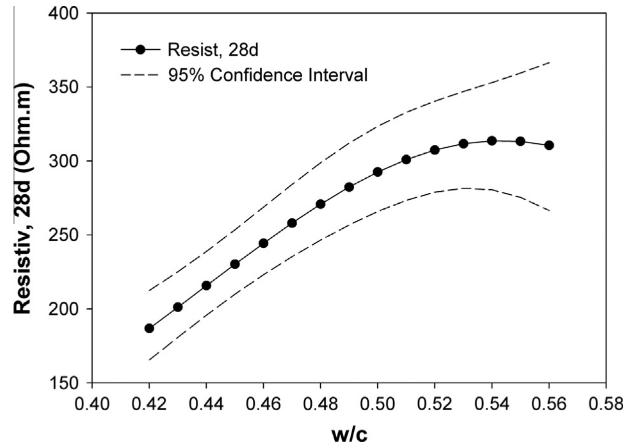

Fig. 9. Estimated values of Resistiv, 28 d (Ω m) for optimized SCC mortars.

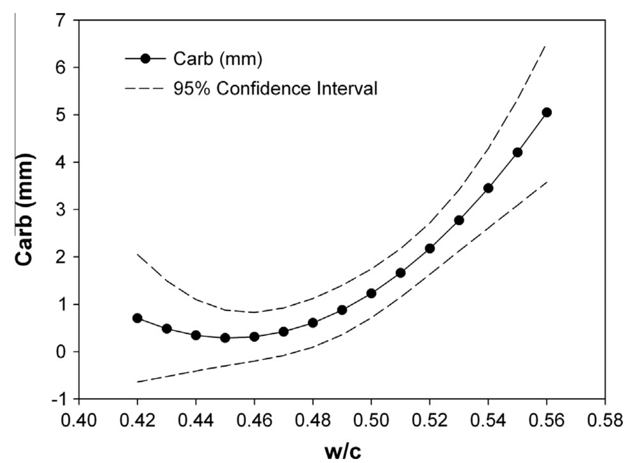

Fig. 10. Estimated values of Carb (mm) for optimized SCC mortars.

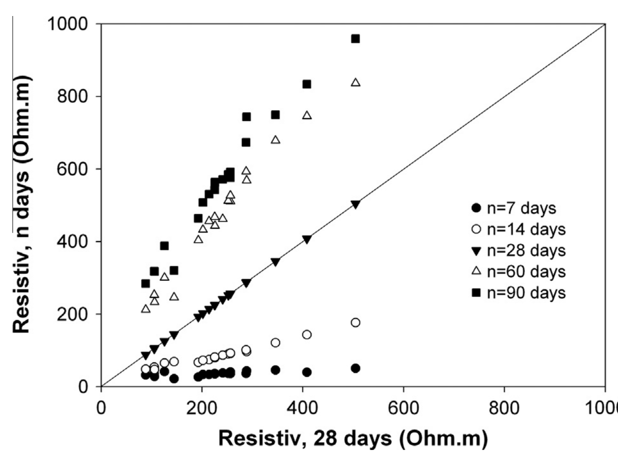

Fig. 11. Evolution of resistivity results with time, for all mixtures in the experimental plan.

to the goals from Eq. (5) (all having equal importance weights) the mix that maximizes the desirability function is: $V_w/V_p = 0.855$; w/c = 0.496 and Sp/p = 1.24%. The corresponding mix-proportions, in terms of kg/m^3, are: $W_c = 487.8$; $W_{GP} = 300.5$; $W_w = 237.7$; $W_{sp} = 9.75$ and $W_s = 1249.2$. The estimated response values for this mix are: Dflow = 260 mm; Tfunnel = 10 s; Resistiv, 28 d = 289 Ω m and Carb, 28 d = 1.1 mm. However, there is uncertainty in the fitted models since they are estimated from a sample of data. In Figs. 9 and 10, uncertainty in the Resistiv, 28 d and Carb, 28 d fitted models is provided for a 95% confidence interval, which depends on the location of the mix in the experimental region. From these figures it can be observed that the selected optimum mix is not located in a zone of larger uncertainty. Concerning fresh state properties, there is a confidence 95% that the intervals (246.9, 273.1) and (9.50, 10.54) contain the true Dflow and Tfunnel for the optimum mix, respectively. In terms of compressive strength (at 28 d), one can expect obtaining results of the same order of magnitude of fc, 28 d results obtained with the current experimental plan (see Table 5).

4.3. Concrete mixture design

SCC concrete mixtures can be obtained by fixing the paste mix proportions given in Section 4.2 and substituting reference sand by common aggregate (one or two fine aggregates and a coarse aggregate). Tests on concrete are then necessary to optimize the aggregate skeleton and aggregate contents. The experimental design technique can also be applied to optimize SCC concrete mixtures considering as independent variables those variables related to the aggregates. Since a high sand content ($V_s/V_m = 0.475$) was selected to optimize mortar mixtures, one can expect obtaining SCCs with higher fine aggregate content and lower paste volume (or higher total aggregates content), thus resulting in more economic mixtures [34].

5. Conclusions

Based on presented results the following conclusions can be drawn:

1. In high performance concrete containing many constituents, where several properties are of interest, it is critical to use a systematic approach to identify optimal mixes given a set of performance constraints. Experimental factorial design provides such an approach.
2. An experimental plan conducted according to a factorial design is useful to evaluate the effects of mixture parameters and their interactions on SCC mortar properties while reducing the number of trial batches needed.
3. Quadratic models provided an adequate representation of each mortar property over the region of interest (namely, flow diameter, V-funnel time, resistivity and carbonation depth) and were used to identify optimal mixes.
4. An increase of GP/c while maintaining w/c (or a decrease of V_w/V_p) strongly influences workability and resistivity of mortar, more than the influence of w/c. It decreases mortar flow diameter and increases both flow time and resisitivity of mortar.
5. Carbonation depth was most influenced by w/c. As expected an increase of w/c, increases carbonation depth.
6. It was shown that ground glass can be successfully applied in SCC mortar, as a high volume cement replacement material, thus widening the types of additions available for SCC, saving landfill and reducing CO_2 emissions by the use of less cement.
7. Results show that fine glass powder enhanced durability, thus providing great opportunities for value adding and cost recovery, by replacing expensive imported materials like silica fume and metakaolin.

In future research, tests will be carried out on the concrete level to further characterize the mechanical, rheological and durability performance when using this material.

Acknowledgments

This work was financed by FEDER funds under the Operational Program Factors of Competiveness – COMPETE and by National Funds under FCT – Foundation for Science and Technology through project PTDC/ECM/098117/2008 – Additions from waste materials for sustainable structural concrete. Acknowledgements are also due to Laboratory of Testing Building Materials (LEMC) and Laboratory for the Concrete Technology and Structural Behaviour (LABEST). Collaboration and materials supplying by SECIL, SIKA is also gratefully acknowledge. We are grateful to the anonymous referees for their helpful comments and suggestions.

References

[1] Mailvaganam NP. Concrete repair and rehabilitation: issues and trends. E-Mat 2004;1(1):1–9.
[2] Mehta PK, Burrows RW. Building durable structures in 21st century. Indian Concr J 2001:437–43.
[3] Tittarelli F, Moriconi G. Use of GRP industrial by-products in cement based composites. Cem Concr Compos 2010;32(3):219–25.
[4] Sousa-Coutinho J. The combined benefits of CPF and RHA in improving the durability of concrete structures. Cem Concr Compos 2003;25(1):51–9.
[5] Garcia ML, Sousa-Coutinho J. Wood Ash from forest waste for partial cement replacement in mortars. Indian Concr J 2008;82(6):39–48.
[6] Garcia ML, Sousa-Coutinho J. Grits and dregs for cement replacement – preliminary studies. In: Walker Peter, Ghavami Khosrow, Paine Kevin, Heath Andrew, Lawrence Mike, Fodde Enrico, editors. Proceedings Nocmat2009 11th international conference on non-conventional materials and technologies materials for sustainable and affordable construction. Bath, UK: University of Bath Press; 2009. <http://opus.bath.ac.uk/16170/1/papers/Paper%20122.pdf>.
[7] Garcia ML, Sousa-Coutinho J. Durability using biomass fly ash as a partial cement replacement. In: Borrás Vicente Amigó, editor. Proceedings II Simposio Aprovechamiento de residuos agro-industriales como fuente sostenible de materiales de construcción (flash card). Valencia, Spain: Editorial Universitat Politècnica de València Press; 2010. p. 25–6 [Book of Abstracts].
[8] Matos AM, Sousa-Coutinho J. Durability of mortars using waste glass powder as cement replacement. Constr Build Mater 2012;36(11):205–15.
[9] Shayan A, Xu A. Value-added utilisation of waste glass in concrete. Cem Concr Res 2004;34(1):81–9.
[10] Liu M. Incorporating ground glass in self-compacting concrete. Constr Build Mater 2011;25(2):919–25.
[11] Shi C, Zheng K. A review on the use of waste glasses in the production of cement and concrete. Resour Conserv Recycl 2007;52(2):234–47.
[12] Xie Z, Xi Y. Use of recycled glass as a raw material in the manufacture of Portland cement. Mater Struct 2002;35(8):510–5.
[13] Chen G, Lee H, Young KL, Yue PL, Wong A, Tao T, et al. Glass recycling in cement production—an innovative approach. Waste Manage 2002;22(7):747–53.
[14] Wang HY, Huang WL. A study on the properties of fresh self-consolidating glass concrete (SCGC). Constr Build Mater 2010;24(4):619–24.
[15] Topçu IB, Canbaz M. Properties of concrete containing waste glass. Cem Concr Res 2004;34(2):267–74.
[16] Terro MJ. Properties of concrete made with recycled crushed glass at elevated temperatures. Build Environ 2006;41(5):633–9.
[17] Shayan A, Xu A. Performance of glass powder as a pozzolanic material in concrete: a field trial on concrete slabs. Cem Concr Res 2006;36(3):457–68.
[18] Taha B, Nounu G. Properties of concrete contains mixed colour waste recycled glass as sand and cement replacement. Constr Build Mater 2008;22(5):713–20.
[19] Bignozzi MC, Saccani A, Sandrolini F. Matt waste from glass separated collection: an eco-sustainable addition for new building materials. Waste Manage 2009;29(1):329–34.
[20] Idir R, Cyr M, Tagnit-Hamou A. Pozzolanic properties of fine and coarse color-mixed glass cullet. Cem Concr Compos 2011;33(1):19–29.
[21] Sobolev K, Türker P, Soboleva S, Iscioglu G. Utilization of waste glass in ECO-cement: strength properties and microstructural observations. Waste Manage 2007;27(7):971–6.
[22] Federico LM, Chidiac SE. Waste glass as a supplementary cementitious material in concrete – critical review of treatment methods. Cem Concr Compos 2009;31(8):606–10.
[23] Shi C, Wu Y, Riefler C, Wang H. Characteristics and pozzolanic reactivity of glass powders. Cem Concr Res 2005;35(5):987–93.
[24] Shao Y, Lefort T, Moras S, Rodriguez D. Studies on concrete containing ground waste glass. Cem Concr Res 2000;30(1):91–100.
[25] Schwarz N, Cam H, Neithalath N. Influence of a fine glass powder on the durability characteristics of concrete and its comparison to fly ash. Cem Concr Compos 2008;30(6):486–96.
[26] Ling TC, Poon CS. Properties of architectural mortar prepared with recycled glass with different particle sizes. Mater Des 2011;32(5):2675–84.
[27] Taha B, Nounu G. Using lithium nitrate and pozzolanic glass powder in concrete as ASR suppressors. Cem Concr Compos 2008;30(6):497–505.

[28] Özkan Ö, Yüksel İ. Studies on mortars containing waste bottle glass and industrial by-products. Constr Build Mater 2008;22(6):1288–98.
[29] Jain JA, Neithalath N. Chloride transport in fly ash and glass powder modified concretes – influence of test methods on microstructure. Cem Concr Compos 2010;32(2):148–56.
[30] Nunes S. Performance-based design of self-compacting concrete (SCC): a contribution to enchance SCC mixtures robustness. PhD thesis. Porto, Faculdade de Engenharia da Universidade do Porto; 2008.
[31] Figueiras H, Nunes S, Sousa-Coutinho J, Figueiras J. Combined effect of two sustainable technologies: Self-compacting concrete (SCC) and controlled permeability formwork (CPF). Constr Build Mater 2009;23(7):2518–26.
[32] Montgomery DC. Design and analysis of experiments. New York: John Wiley & Sons; 2001.
[33] Okamura H, Ozawa K, Ouchi M. Self-compacting concrete. Struct Concr 2000;1:3–17.
[34] Nunes S, Milheiro-Oliveira P, Sousa-Coutinho J, Figueiras J. Interaction diagrams to assess SCC mortars for different cement types. Constr Build Mater 2009;23(3):1401–12.
[35] Rajabipour F, Weiss J. Electrical conductivity of drying cement paste. Mater Struct 2007;40(10):1143–60.
[36] Andrade C. Calculation of initiation and propagation periods of service life of reinforcement by using the electrical resistivity. In: Weiss J, Kovler K, Marchand J, Mindess S, editors. Proceedings first international RILEM symposium on advances in concrete through science and engineering. Evanston, Illinois: RILEM Publications SARL; 2004. p. 23–30.
[37] Shi C, Stegemann JA, Caldwell RJ. Effect of supplementary cementing materials on the specific conductivity of pore solution and its implications on the rapid chloride permeability test (AASHTO T277 and ASTM C1202) results. ACI Mater J 1998;95(4):389–94.
[38] Figueiras H, Nunes S, Sousa-Coutinho J, Figueiras J. Durability performance of SCC mortars including different types of metakaolin. In: Freitas VP, Corvacho H, Lacasse M, editors. Proceedings 12th international conference on durability of building materials and components. Porto, Portugal: FEUP edições; 2011. p. 1387–94.
[39] Especificação LNEC E 361:1993. Determinação da resistência à carbonatação. Lisboa (Portugal) [in Portuguese].
[40] State-Ease Corporation. Design-Expert Software, Version 6 Useŕs Guide; 2000.